Carbohydrate Polymers 89 (2012) 282–289

Contents lists available at SciVerse ScienceDirect

Carbohydrate Polymers

journal homepage: www.elsevier.com/locate/carbpol

Chitosan/carrageenan nanoparticles: Effect of cross-linking with tripolyphosphate and charge ratios

Susana Rodrigues[a], Ana M. Rosa da Costa[b], Ana Grenha[a,*]

[a] CBME – Centre for Molecular and Structural Biomedicine/IBB – Institute for Biotechnology and Bioengineering, University of Algarve, Faculty of Sciences and Technology, Campus de Gambelas, 8005-139 Faro, Portugal
[b] CIQA – Centre of Research in Chemistry of Algarve, Faculty of Sciences and Technology, Campus de Gambelas, 8005-139 Faro, Portugal

ARTICLE INFO

Article history:
Received 3 January 2012
Received in revised form 28 February 2012
Accepted 1 March 2012
Available online 8 March 2012

Keywords:
Chitosan
Cross-linking
k-Carrageenan
Nanoparticles
Tripolyphosphate

ABSTRACT

Chitosan/carrageenan/tripolyphosphate nanoparticles were prepared by polyelectrolyte complexation/ionic gelation, the latter compound acting as cross-linker. The incorporation of the three components in the nanoparticle matrix was assessed by analytical techniques (FTIR, XPS and TOF-SIMS).

Using chitosan/carrageenan nanoparticles as control, the effect of the cross-linker in the particles properties was studied. A decrease in size (from 450–500 nm to 150–300 nm) and in zeta potential (from +75 – +85 mV to +50 – +60 mV), and an increase in production yield (from 15–20% to 25–35%), and in stability (from one week to up to 9 months) were observed. Also, a correlation between positive to negative charge ratios in the formulations and the above characteristics was established.

The small size and high positive surface charge make the developed chitosan/carrageenan/tripolyphosphate nanoparticles potential tools for an application in mucosal delivery of macromolecules.

1. Introduction

Polymeric nanoparticles have been used increasingly in various fields, such as drug delivery, imaging and tissue engineering, the first being, by far, the most reported application. The main reason justifying the widespread use of polymeric nanoparticles relies on the displayed high surface-to-volume ratio which improves the loading capacity of the selected molecule, while providing its protection. In addition, increased drug absorption might be attained by the capacity of nanoparticles to reduce epithelial resistance to transport (de la Fuente, Csaba, Garcia-Fuentes, & Alonso, 2008; Rawat, Singh & Saraf, 2006; Reis and Ribeiro, 2006).

Many polymers have been used to prepare these vehicles, but those of natural origin are often preferred because, as compared to synthetic counterparts, they comply more easily with the requisites of biocompatibility, biodegradability and absence of toxicity that are mandatory in any biomedical application (Liu, Jiao, Wang, Zhou & Zhang, 2008; Malafaya, Silva & Reis, 2007). Chitosan (CS) and carrageenan (CRG) are two marine-derived polymers which belong to the above mentioned class, and have demonstrated in a previous study the ability to assemble into nanoparticles of 400–600 nm (Grenha et al., 2010). CS is a cationic polysaccharide composed of repeating units of *N*-acetylglucosamine and D-glucosamine that are β-(1–4)-linked (Fig. 1), and presents well-documented favorable properties for drug delivery such as biocompatibility, biodegradability, low toxicity (Dornish, Hagen, Hansson, Peucheur, Vedier & Skaugrud, 1997; Hirano, Seino, Akiyama & Nonaka, 1988) and mucoadhesiveness (Lehr, Bouwstra, Schacht & Junginger, 1992). CRG is another polysaccharide, extracted from red seaweed (van de Velde, Knutsen, Usov, Rollemay, & Cerezo, 2002) and composed of galactose and anhydrogalactose units, linked by glycosidic bonds (Fig. 1) (Lim, Gwon, Choi, Shin & Nho, 2010). Due to its half-ester sulfate moieties, carrageenan displays a strong ionic nature and exhibits a high capacity to react with proteins (Malafaya et al., 2007; Mohamadnia, Zohuriaan-Mehr, Kabiri, Jamshidi & Mobedi, 2007). There are two types of carrageenan that evidence gel-forming ability, *k*- and *i*-, *k*-carrageenan gels being more firm than those obtained with *i*-carrageenan, which are more elastic and soft (Bixler, 1993). The assembly of the referred CS/CRG nanoparticles was mediated by polyelectrolyte complexation (Grenha et al., 2010), a method that uses very mild conditions, avoiding harmful organic solvents or high shear forces. Therefore, it has the general capability of protecting the encapsulated molecules and retaining their activity during the encapsulation, which are its principal advantages (Mohanraj and Chen, 2006; Saboktakin, Tabatabaie, Maharramov & Ramazanov, 2010; Grenha, 2012). This methodology involves the interaction between a chitosan with high degree of protonation and a polyanion, permitting the rapid formation of

* Corresponding author at: Centre for Molecular and Structural Biomedicine (CBME), Faculty of Sciences and Technology, Building 8, Room 2.4, Campus de Gambelas, 8005-139 Faro, Portugal. Tel.: +351 289800100x7441; fax: +351 289 818419.
E-mail address: amgrenha@ualg.pt (A. Grenha).

0144-8617/$ – see front matter © 2012 Elsevier Ltd. All rights reserved.
doi:10.1016/j.carbpol.2012.03.010

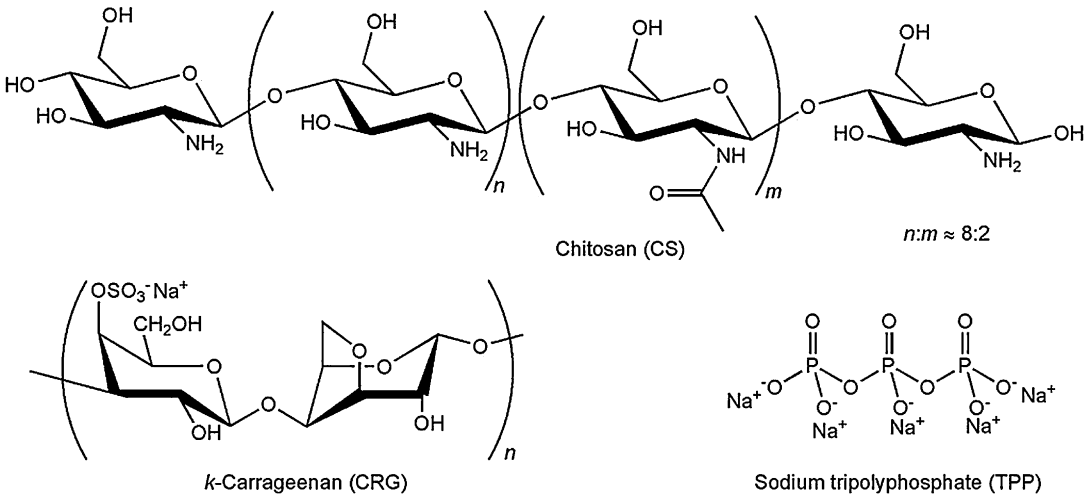

Fig. 1. Chemical structures of materials composing the matrix of nanoparticles: chitosan, *k*-carrageenan and sodium tripolyphosphate.

nanoparticles. Their size, as well as other characteristics, might be modulated by adjusting formulation parameters like the type of materials composing the particles matrix, their concentration and mass ratios, amongst others (Calvo, Remuñán-López, Vila-Jato, & Alonso, 1997a; Grenha, 2012).

In many cases, for instance if the nanoparticles are to be applied in mucosal delivery, it is important to ensure that their size will permit the contact with the epithelial surface, an effect that is maximised for particles between 50 nm and 500 nm (Desai, Labhasetwar, Amidon & Levy, 1996; Jani, Halbert, Langridge & Florence, 1990). Preparing nanoparticles in this size range is facilitated by the use of adequate cross-linking agents. Tripolyphosphate (TPP) is a non-toxic polyanion (Fig. 1) known for its capacity to cross-link chitosan, a reaction mediated by electrostatic forces, resulting in the formation of ionic cross-linked networks (Janes, Calvo & Alonso, 2001; Mi, Sung, Shyu, Su & Peng, 2003).

The objective of this work was to produce CS/CRG nanoparticles, including in the formulation TPP as cross-linking agent, and to evaluate the effect of the presence of this polyanion on the properties of nanoparticles, namely concerning size, surface charge and stability. To do so, different amounts of cross-linker were used and formulations with different polymeric mass ratios were tested. Reduced size and strong positive surface charge would improve the nanoparticles contact with mucosal epithelial surfaces, which is very positive when considering an application in mucosal drug delivery.

2. Experimental

2.1. Materials

Chitosan (low molecular weight, deacetylation degree = 75–85%), pentasodium tripolyphosphate, glycerol and glacial acetic acid were supplied by Sigma Chemicals (Germany). *k*-carrageenan and potassium bromide (KBr) were obtained from FMC Biopolymer (Norway) and Riedel-del-Haën (Germany), respectively. Ultrapure water (Milli-Q Plus, Millipore Iberica, Spain) was used throughout.

2.2. Nanoparticles preparation

CS/CRG/TPP nanoparticles were prepared by a modification of a previously described methodology (Grenha et al., 2010), based on the polyelectrolyte complexation of CS with CRG and additional ionic gelation of chitosan with TPP anions. Briefly, CS was dissolved in 1% (w/w) acetic acid to obtain a solution of 1 mg/mL and CRG and TPP were dissolved in purified water to obtain stock solutions of 2.5 and 10 mg/mL, respectively. Different volumes of the latter solutions were mixed in order to obtain volumes of 0.8 mL of solutions with the required concentrations of both components. The spontaneous formation of nanoparticles occurs upon incorporation, under gentle magnetic stirring at room temperature, of the aforementioned solutions into 2 mL of the CS solution, corresponding to final theoretical CS/CRG/TPP ratios varying from 4/1/0 to 7/1/1 (w/w).

Nanoparticles were concentrated by centrifugation at 16,000 × *g* on a 10 μL glycerol layer for 30 min at 15 °C (centrifuge 5804R, Eppendorf, Germany). The supernatants were discarded and nanoparticles were ressuspended in 200 μL of purified water.

2.3. Nanoparticles physicochemical characterization

The production yield of nanoparticles was calculated by gravimetry. Fixed volumes of nanoparticle suspensions were centrifuged (16,000 × *g*, 30 min, 15 °C), and sediments were freeze-dried over 24 h at −34 °C, followed by a gradual increase in temperature until 20 °C, using a Labconco freeze dryer (Labconco, USA) ($n = 3$).

The process yield (P.Y.) was calculated as follows: P.Y. (%) = (nanoparticle sediment weight/total solid weight) × 100.

The morphological examination of CS/CRG/TPP nanoparticles was conducted by transmission electron microscopy (TEM) (JEM-1011, JEOL, Japan). The samples were stained with 2% (w/v) phosphotungstic acid and placed on copper grids with Formvar® films for TEM observation.

Measurements of nanoparticle size and zeta potential were performed on freshly prepared samples by photon correlation spectroscopy and laser Doppler anemometry, respectively, using a Zetasizer Nano ZS (Malvern Instruments, Malvern, UK). For the analysis of particle size and determination of the electrophoretic mobility, each sample was diluted to the appropriate concentration with ultrapure water and placed in the electrophoretic cell. Each analysis was performed at 25 °C. Three batches of each formulation were analyzed ($n = 3$).

2.4. Nanoparticle stability study

Aliquots of nanoparticle formulations with and without TPP (formulations 5/1/1 and 5/1/0, respectively) were stored at 4 °C. Nanoparticle sizes and zeta potentials were monitored as a function of time for 250 days, using the technique described above ($n = 3$).

2.5. Nanoparticles chemical analysis

2.5.1. Fourier transform infrared (FTIR) spectroscopy

The interactions between the different components of the nanoparticulate systems were analyzed by FTIR. Infrared spectra of the specimen powders, namely CS, CRG and TPP, and CS/CRG/TPP nanoparticles (formulation 5/1/1), were recorded using a FTIR spectrophotometer (Tensor 27, Bruker, Germany). Prior to the assay, the samples were gently triturated with KBr and compressed into discs.

For each spectrum a 32-scan interferogram was collected in transmittance mode with a 4 cm^{-1} resolution in the 4000–400 cm^{-1} region at room temperature.

2.5.2. Surface analysis by X-Ray photoelectron spectroscopy (XPS) and time-of-flight secondary ion mass spectrometry (TOF-SIMS)

The surface of CS/CRG/TPP nanoparticles was analyzed to determine their chemical composition. To do so, a droplet of nanoparticles (formulations 4/1/1 and 5/1/1) was placed directly on a polished monocrystalline silicon wafer, used as a sample holder. The droplet was then allowed to dry in a desiccator, prior to the analyses. The surface of the samples was analyzed by XPS (K-Alpha ESCA, Thermo Scientific, UK) and TOF-SIMS (TOF-SIMS IV, Ion-TOF GmbH, Germany). Solutions of the different compounds (CS, CRG and TPP) were analysed separately as controls.

The XPS measurements were carried out using monochromatic Al-Ka radiation ($h\nu$ = 1486.6 eV), and photoelectrons were collected from a take-off angle of 90° relative to the sample surface. The X-ray monochromatic spots were 400 μm in diameter and the correspondingly sampling area was 0.1256 mm^2. Measurements were performed in constant analyzer energy (CAE) mode with 100 eV pass energy for survey spectra and 20 eV pass energy for high-resolution spectra. Charge referencing was done by setting the lower binding energy C 1s photopeak at 285.0 eV, the C 1s hydrocarbon peak (Briggs and Seah, 1983). Surface elemental composition was determined using the standard Scofield photoemission cross section. Residual vacuum in the analysis chamber was maintained at around 3×10^{-9} mbar.

For TOF-SIMS analyses, samples were bombarded with a pulsed bismuth ion beam (Bi^{3+}) generated with a liquid metal ion gun operated at 25 keV and a 45° incidence with respect to the sample surface. The secondary ions generated were extracted with a 10 kV voltage, and their time-of-flight from the sample to the detector was measured in a reflectron mass spectrometer. Electron flood gun charge compensation was necessary during measurements. A raster size of 500 μm × 500 μm was used, and at least three different spots were analyzed under the "static" condition with ion doses of 2×10^{12} ions/cm^2. The calibration of the mass spectra in the positive mode was based on hydrocarbon peaks such as CH_3^+, $C_2H_3^+$, $C_3H_5^+$ and $C_7H_7^+$. Negative spectra were calibrated to the C^-, C_2^-, C_3^-, C_4^-, C_2H^-, C_3H^- and C_4H^- peaks before further analysis. The experimental conditions (ion type, beam voltage, and primary ion dose) were maintained constant for each experiment.

2.6. Statistical analysis

The *t*-test and the one-way analysis of variance (ANOVA) with the pair wise multiple comparison procedures (Student–Newman–Kleus Method) were performed to compare two or multiple groups, respectively. All analyses were run using the SigmaStat statistical program (Version 3.5, SyStat, USA) and differences were considered to be significant at a level of $p < 0.05$.

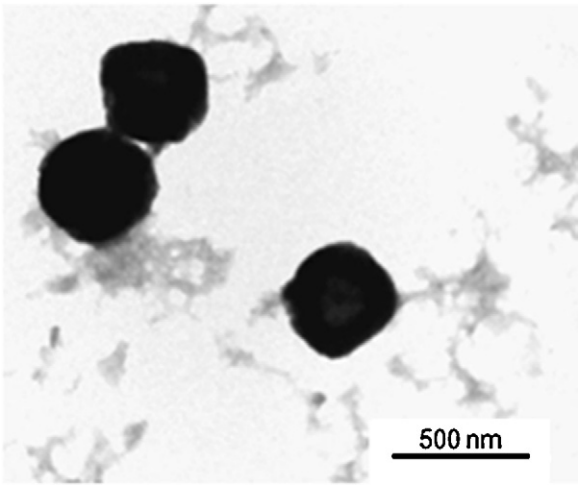

Fig. 2. TEM microphotograph of representative CS/CRG/TPP (4/1/1) nanoparticles.

3. Results and discussion

3.1. CS/CRG/TPP nanoparticles characterization

CS/CRG/TPP nanoparticles were produced by a very mild polyelectrolyte complexation/ionic gelation method, as described in the Experimental Section. Briefly, when the three components are mixed, an electrostatic interaction is established between the positively charged amino groups of CS and the negatively charged sulphate and phosphate groups of CRG and TPP, respectively, leading to the nanoparticle formation in a process derived from inter- and intramolecular linkages mediated by the anionic molecules (Janes et al., 2001). TPP affords a further intense interaction, as it provides a cross-linking effect. Fig. 2 displays a TEM microphotograph of representative CS/CRG/TPP nanoparticles, showing a spherical morphology and compact structure.

An estimation of the positive to negative (+/−) charge ratios for the different formulations was made, based on the following assumptions: (1) Chitosan was considered to have one positive charge per deacetylated monomer and, since it has a deacetylation degree of 75–85%, a mean value of 0.8 positive charges per monomer was used. According to a reported method (Ma et al., 2008) an average monomeric molecular weight of 169 g/mol for this deacetylation degree was obtained; (2) Carrageenan was assumed to be in the sodium salt form, to which corresponds a mass of 408 g/mol and a negative charge per disaccharide monomer unit; (3) Pentasodium tripolyphosphate has a molar mass of 368 g/mol and five negative charges per anion. The mass of each compound in every formulation was then converted to moles of charge and the +/− molar ratio was calculated.

As can be seen in Fig. 3, formulations with mass ratios below 4/1/1 (as 2/1/0.5 and 3/1/1), which evidence a +/− charge ratio around 1 (Fig. 3A), resulted in precipitation (Fig. 3B). The observed precipitation for lower ratios is due to the presence of an excess of anionic charges, which neutralize chitosan positive charges and, thus, reduce or eliminate electrostatic repulsion, leading to precipitation. In fact, a 1:1 +/− charge stoichiometry does not mean that complete charge neutralization will occur, due to different charge spacings in the intervenient species and to steric constraints. However, one may assume a preferential interaction between the sulphate and the ammonium groups, both weakly hydrated, instead of with the strongly hydrated counterions (Crouzier and Picart, 2009). The same assumption should apply to TPP polyanion. This would lead to mainly an intrinsic charge matching in detriment of

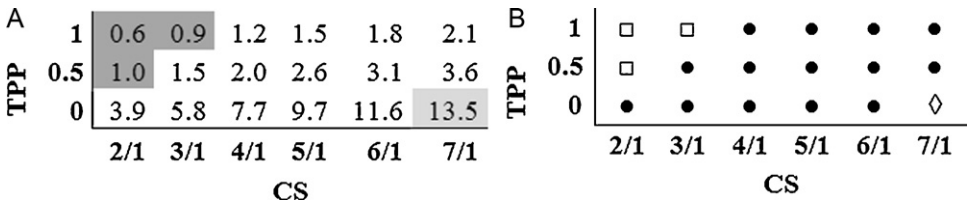

Fig. 3. Representative scheme of (A) positive/negative charge ratio of each formulation (white fill: formation of nanoparticles; dark grey: precipitation; light grey: inability to form nanoparticles). (B) the ability to form nanoparticles according to formulation composition: precipitation (□); nanoparticles (●); solution (◊).

an extrinsic charge compensation and, thus, to a small deviation from neutrality.

On the contrary, the formulation corresponding to a mass ratio of 7/1/0, which displays a +/− charge ratio of 13.5, did not lead to nanoparticle formation. As observed by other authors and, according to the described formation mechanism of nanoparticles, which is mediated by electrostatic interactions, the absence of nanoparticle formation is attributed to an insufficient number of anionic charges to neutralise CS amino groups (Calvo et al., 1997a; Fernández-Urrusuno, Calvo, Remuñán-López, Vila-Jato & José Alonso, 1999). For this reason, Fig. 4 only depicts the physicochemical characteristics of CS/CRG/TPP nanoparticles of mass ratios between 4/1/0 and 6/1/1.

Observing in Fig. 4A the data corresponding to formulations containing only CS/CRG (4/1/0–6/1/0), no significant differences are observed for both size and zeta potential, which lay around 450–500 nm and +80 mV, respectively. However, bearing in mind the observations of Fig. 3A, concerning charge ratios, there is a tendency to decrease the size from the formulation 4/1/0 (charge ratio of 7.7) to 6/1/0 (charge ratio of 11.6), which is attributed

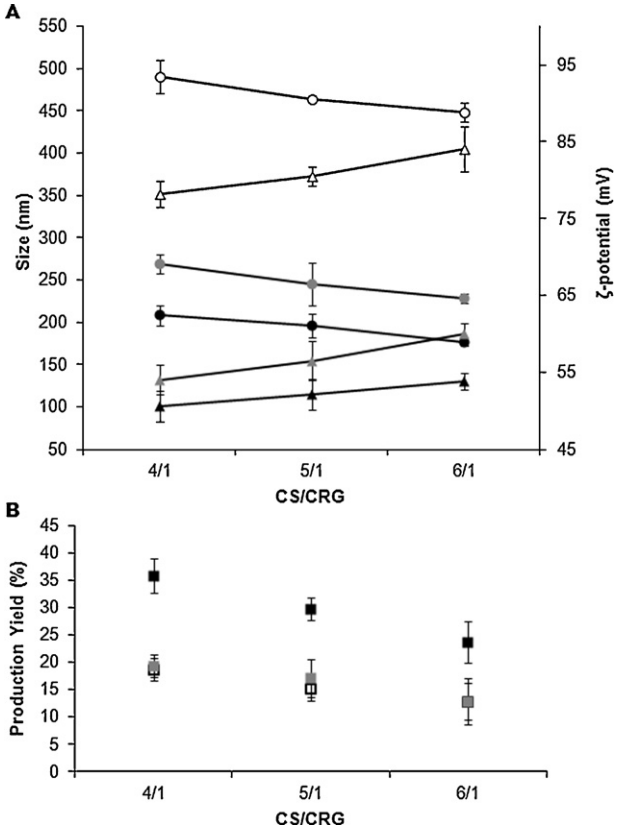

Fig. 4. Effect of CS/CRG mass ratio and TPP amount on (A) nanoparticle size (round marks) and zeta potential (triangular marks) and (B) production yield of nanoparticle (square marks). White: 0 TPP; grey: 0.5 TPP; black: 1 TPP (mean ± SD, $n = 3$).

to the increase in the charge ratio, as reported elsewhere (Chen, Mohanraj, Wang & Benson, 2007; Nizri, Magdassi, Schmidt, Cohen & Talmon, 2004; Nizri, Makarsky, Magdassi & Talmon, 2009). Increasing CRG content in the formulation (from 6/1/0 to 4/1/0) leads to a lower charge ratio due to the negative charge of CRG sulphate groups. This resulted, as expected, in a zeta potential decrease. Comparing these data with some reported previously for CS/CRG nanoparticles (Grenha et al., 2010), we observe similar tendencies but smaller nanoparticle sizes in the present work for comparable formulations, which might be explained by the use of chitosan and carrageenan from different suppliers (van de Velde et al., 2002). In Fig. 4B it is seen that the production yields are relatively low (13–19%) and comparable in all cases. In the present study, CS/CRG nanoparticles were used as control.

The incorporation of TPP in the matrix of nanoparticles succeeded in providing an effective cross-linking effect. More specifically, the presence of TPP resulted in alterations on all the typical characterization parameters, namely the nanoparticle size and zeta potential (Fig. 4A), as well as production yield (Fig. 4B). For the highest amount of TPP incorporated (mass ratio of 1 compared to chitosan), particle size decreased to 176–208 nm ($p < 0.05$) and zeta potential also decreased from +80 mV to approximately +50 mV ($p < 0.05$). Size decrease is attributed to the cross-linking effect, which induces the condensation of polymeric chains, resulting in smaller particles. The simultaneous decrease in zeta potential is a consequence, not only of the inclusion of a negatively charged material in the matrix of nanoparticles, but also of the general size decrease, which possibly exposes a lower number of charged groups because of the diminished surface. Interestingly, it can be observed that the incorporation of a mass ratio of only 0.5 of TPP is enough to induce a clear effect on size and zeta potential, but a higher amount of cross-linking agent (mass ratio of 1 compared to chitosan) is necessary to produce a significant effect on production yield ($p < 0.05$). In fact, if the formulation 4/1 is considered as example, it is seen by observation of Fig. 4 that the addition of 0.5 TPP does not modify the production yield, but it significantly decreases both the nanoparticles size, by 45% (from 491 nm to 269 nm), and the zeta potential, by 25% (from +78 to +54 mV). A further increase of 0.5 TPP, resulting in a final CS/CRG/TPP = 4/1/1, results in a significant increase of the production yield to 36%, while the changes in the size and zeta potential, although significant ($p < 0.05$), are not very pronounced, as size decreases 61 nm and zeta potential 4 mV. This trend was similarly observed for the remaining formulations and, in all cases, the polydispersity index was lower than 0.3. The inclusion of TPP in the nanoparticles was also observed to result in unimodal size distribution.

The production yield practically doubled in all formulations with the highest amount of TPP ($p < 0.05$), reaching a maximum of 36% for CS/CRG/TPP = 4/1/1. This behaviour could be explained by the specific mechanism of nanoparticle formation, according to which a determined amount of negative charges is necessary to provide a certain degree of neutralisation of chitosan amino groups, which leads to the formation of nanoparticles. When adding 0.5 TPP the cross-linking occurs, decreasing the size of nanoparticles, but the amount of phosphate groups is not enough to increase the

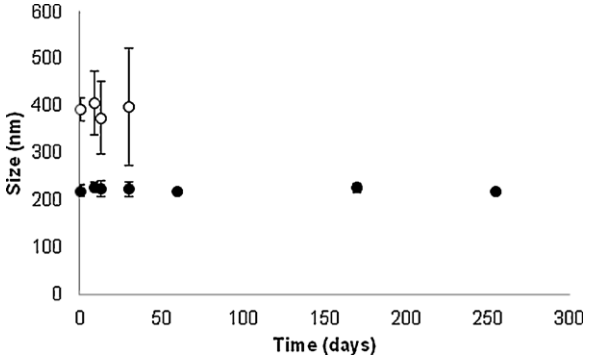

Fig. 5. Evolution of CS/CRG (○) and CS/CRG/TPP (●) nanoparticle size as a function of time, upon storage at 4 °C (mean ± SD, $n = 3$).

number of formed nanoparticles, an effect that is observed when TPP amount is doubled. The obtained results are in accordance with the ability of TPP to cross-link chitosan, demonstrating in this case the capacity to decrease the size of chitosan-based nanoparticles obtained by polyelectrolyte complexation with another polymer.

These results demonstrate, as a whole, that the charge ratio plays a critical role in the production of nanoparticles by electrostatic interactions. In fact, it is shown that the final properties of CS/CRG/TPP nanoparticles can be adjusted by modulating charge ratios.

3.2. Nanoparticles stability study

The data corresponding to nanoparticles size evolution over time is depicted in Fig. 5, for formulation CS/CRG/TPP = 5/1/1 and for the corresponding CS/CRG formulation, which was used as control. The rationale of conducting this assay in water was the interest in obtaining information on the nanoparticles stability in the resuspension medium. In the cases where the nanoparticles are an intermediate product of the final drug delivery system, as reported in some works of our group (Grenha, Seijo, Serra & Remuñán-López, 2007; Al-Qadi, Grenha & Remuñán-López, 2011), this could avoid the need of extra procedures to stabilize the nanoparticles, as a lyophilization step for instance.

The formulation without TPP tends to demonstrate some degree of size variation, although not statistically significant, accompanied by an increase in the polydispersity after 7 days of storage. On the contrary, the formulation containing TPP evidenced improved stability, without signals of significant size variation during the experimental period of 250 days. Zeta potential was also monitored in this study, but no alterations were found over time for either of the assayed formulations (data not shown). Other authors reported the stability of CS/TPP nanoparticles when stored at 5 °C for 15 days in non-buffered medium, further observing an increase in the polydispersity after that period, as the standard deviation of mean size of the nanoparticles registered a significant increase (López-León, Carvalho, Seijo, Ortega-Vinuesa & Bastos-González, 2005). The results found in the present study for the CS/CRG/TPP formulation indicate that TPP acts as a stabiliser, possibly because of its cross-linking effect, which causes polymeric molecules to establish stronger interactions with each other to form a more stable structure, less prone to aggregation. Actually, cross-linking reactions have been described to improve the properties of particulates (Mi et al., 2003), hydrogels (Sung, Huang, Chang, Huang & Hsu, 1999) and scaffolds (Adekogbe and Ghanem, 2005), amongst other structures.

Table 1
Surface composition (atomic percentage) determined by XPS of CS, CRG, TPP and CS/CRG/TPP nanoparticles of different ratios.

Element	CS (%)	CRG (%)	TPP (%)	4/1/1 NP (%)	5/1/1 NP (%)
C	64.1	57.4	16.0	57.5	57.9
O	29.6	38.2	63.6	35.2	35.1
N	6.3	1.1	0	4.0	4.0
P	0	0	20.4	2.0	1.7
S	0	3.3	0	1.3	1.3
Ratio O/N	4.69	35.7	0	8.75	8.73
Ratio C/N	10.2	53.6	0	14.3	14.4

CS, chitosan; CRG, carrageenan; NP, nanoparticles; TPP, tripolyphosphate.

3.3. Chemical analysis of nanoparticles

As commented above, formulations containing TPP showed different physicochemical characteristic as compared to those without TPP, which suggests that TPP is in fact incorporated in the matrix of nanoparticles. Nevertheless, an indubitable demonstration of TPP presence is possible only by chemical analysis of the formulations. In this manner, specific techniques of chemical analysis, such as FTIR, XPS and TOF-SIMS, were used to characterize the chemical composition of nanoparticles, the last two techniques referring to surface analysis.

3.3.1. FTIR analysis

The FTIR spectrum of CS/CRG/TPP nanoparticles is depicted in Fig. 6, along with the spectra of all the materials separately (CS, CRG and TPP), which were used as controls in this assay. TPP spectrum presents two intense absorption bands at 1147 and 906 cm^{-1}, attributed, respectively, to P═O and P–O along with P–O–P. The overlapping of the former with the sulphate band of *k*-carrageenan (van de Velde et al., 2002) and of the latter with the carbohydrate bands, renders the detection of their presence in the nanoparticles ambiguous. Moreover, those bands are expected to shift upon protonation and hydrogen bonding (Jiang, Saxena, Song, Ward, Beveridge & Myneni, 2004), which may occur during particle formation. However, the collapse of the sulphate and polysaccharide bands observed in the nanoparticles may be accounted for if TPP is present, especially if shifting of the 1147 cm^{-1} band occurred. Also, the band at 894 cm^{-1} in the nanoparticles may be attributed to a shift in the 906 cm^{-1} band of TPP. The amide bands are masked by the 1644 cm^{-1} bending band of adsorbed water (Wilson, Smith, Kacurakova, Saunders, Wellner & Waldron, 2000) and the new 1539 cm^{-1} absorption of the amino groups in protonated CS.

3.3.2. Surface analysis by XPS and TOF-SIMS

XPS is one of the most commonly used techniques of surface analysis. Upon exposure of the sample to an X-ray beam, the binding energies of characteristically emitted photoelectrons are measured, providing information on the elements from which they originate, as well as their chemical bonding. Table 1 displays the percentage of each chemical element present in the sample of either controls (CS, CRG and TPP) or nanoparticles. The final chemical composition of a sample can be obtained from core photoemission intensity peak areas using the Shirley background subtraction technique from the survey spectra. The element composition can be quantified by using X-ray photoelectron intensity values and the Scofield theoretically derived set of atomic sensitivity factors. Some of the samples showed an intensive silicon signal (data not shown), which is attributed to the substrate, as a consequence of an incomplete coating of the substrate surface with the sample. These Si signals do not compromise the obtained results and are not included in Table 1. The survey of controls detected the expected elements, such as carbon (C), oxigen (O), nitrogen (N), phosphorus (P) and sulfur (S). The obtained CS composition (64.1% C, 29.6% O

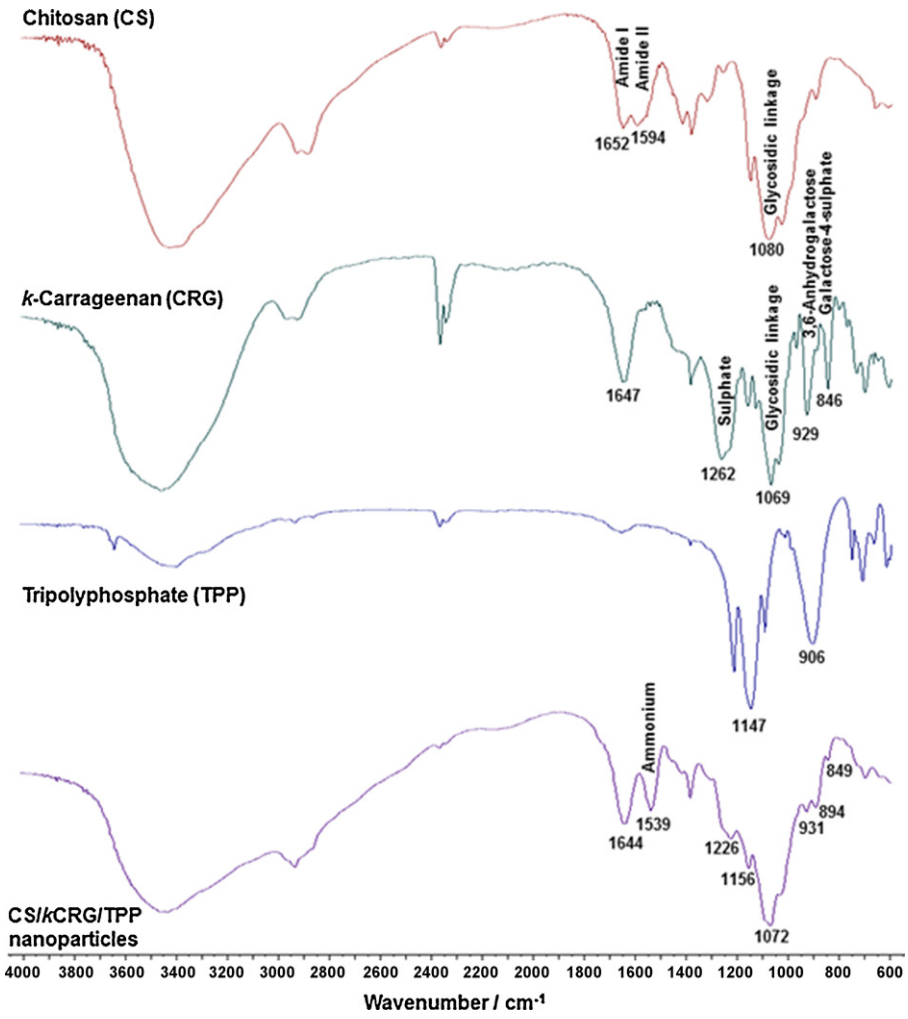

Fig. 6. FTIR spectra of CS, CRG, TPP and CS/CRG/TPP (5/1/1) nanoparticles.

and 6.3% N) is similar to that observed by Silva et al., who used the same CS type to produce membranes and obtained 66.4% C, 28.0% O and 5.6% N. In addition, these authors report an O/N ratio of 4.98, which is close to that of the present work (4.69) (Silva et al., 2008).

In this work, the prepared nanoparticles were found to contain approximately 57% C, 35% O, 4% N, 2% P and 1% S, the content of P being necessarily attributed to the cross-linking agent TPP, and that of S having origin in CRG. The obtained atomic percentages of C, O, N and P were comparable to those reported in other works for the analysis of CS/TPP nanoparticles (53.8% C, 33.8% O, 4.5% N and 2.7% P) (Calvo, Remuñán-López, Vila-Jato, & Alonso, 1997b; Grenha et al., 2007). The slight variations can be explained by the use of CS of different characteristics and the analysis of nanoparticles with different compositions and mass ratios. The C/N ratio of nanoparticles assayed in the present study (14.3) is slightly higher than those reported by Grenha et al. (11.9)(Grenha et al., 2007) and Calvo et al. (10.9)(Calvo et al., 1997b). This difference is attributed to the presence of an extra compound in the nanoparticles formulation (CRG), which increased the amount of C, thereby increasing the C/N ratio.

Unexpectedly, a certain amount of C and N were detected in the TPP and CRG samples, respectively. This effect was reported by other authors as corresponding to the atmospheric exposure of the samples, which led to the adsorption of some adventitious carbon (Barr and Seal, 1995; Swift, 1982) and nitrogen (Allott, Curtis, Hall, Harriman & Battarbee, 1995; Baltrusaitis, Jayaweera & Grassian, 2009; Edwards, Zak, Kellner, Eisenlord & Pregitzer, 2011; Rao, Rao & Ppabhakaran, 1987) on the samples surface.

In contrast to photoelectron spectroscopy techniques such as XPS, TOF-SIMS not only provides information on the elements present on analysed surfaces, but also offers detailed molecular information with high sensitivity. This technique has been useful in the characterization of surface chemistry of pharmaceutical systems (Barnes, Kempson & Prestidge, 2011). Fig. 7 displays the negative mass spectra, between 50 and 110 mass/u, obtained by TOF-SIMS for each of the analysed samples.

The spectrum of CS (Fig. 7A) evidences a peak at m/z 58 corresponding to C_2H_4NO (Al-Qadi et al., 2011), as well as peaks at m/z 59 ($C_2H_3O_2$), 69 (C_3HO_2), and 71 ($C_3H_3O_2$). Typical fragments of chitosan were also detected in the sample of control chitosan, such as $C_{14}H_9NO$, $C_4H_{21}N_{14}O$ and $C_8H_{15}NO_6$ (data not shown), the latter representing one of the typical units of chitosan molecule, *N*-acetyl-D-glucosamine (Grenha, Remuñán-López, Carvalho & Seijo, 2008; Grenha et al., 2007). The CRG spectrum (Fig. 7B) is dominated by SO_2, SO_3 and SO_4H peaks, at m/z 64, 80 and 97, respectively. Smaller peaks, attributed to saccharide species, as well as to SO_4, are also present. TPP spectrum (Fig. 7C) consists of two peaks, corresponding to PO_2 and PO_3, at m/z 63 and 79 (Al-Qadi et al., 2011).

As it is demonstrated in Fig. 7C and D, the mass spectra of both nanoparticle formulations evidence peaks that are characteristic of all the previous spectra, which correspond to controls. The obtained results are in agreement with those previously observed in the XPS analysis, indicating the presence of all the components (CS, CRG and TPP) in the nanoparticles and suggesting a homogeneous distribution of the various constituents through their matrix.

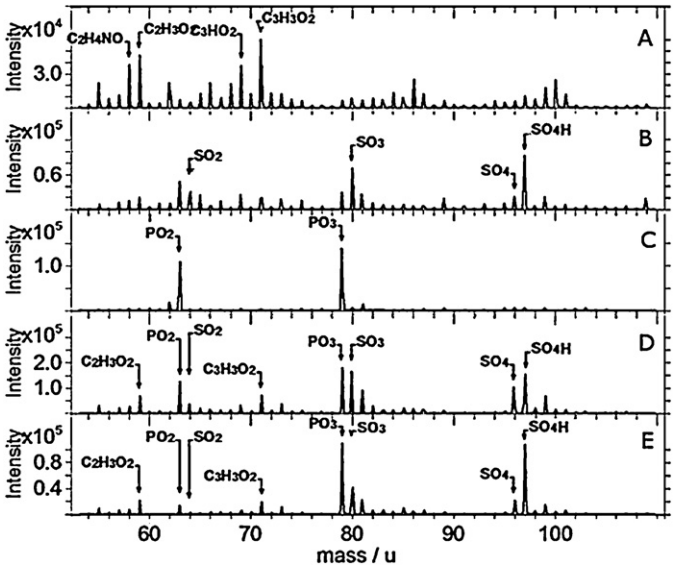

Fig. 7. Negative ion mass spectra obtained by TOF-SIMS analysis of (A) CS, (B) CRG, (C) TPP, (D) CS/CRG/TPP = 4/1/1 nanoparticles and (E) CS/CRG/TPP = 5/1/1 nanoparticles.

However, given the novelty of this technique, few references were found reporting results of the application of TOF-SIMS on similar materials and those found report fragment peaks with higher masses (mass/u), thus, the establishment of comparisons with previously developed works was very scarce.

4. Conclusions

In this work, nanoparticles comprising CS, CRG and TPP were produced and characterized using several techniques such as photon correlation spectroscopy and laser Doppler anemometry, TEM, FTIR, XPS, and TOF-SIMS. The three components were identified in the FTIR, XPS and TOF-SIMS spectra of the nanoparticles, thus indicating an effective association of all the materials. In particular, their detection by the surface analysis techniques suggests a homogeneous distribution through the nanoparticles' matrix.

TPP acted as a cross-linker agent and, therefore, enabled the production of nanoparticles with smaller size, apart from increasing their production yield. In addition, the presence of TPP in the nanoparticle matrix increased their stability, providing a shelf-life of at least 9 months. Charge ratios were demonstrated to play a critical role in the nanoparticles formation, since a ratio around 1 leads to precipitation, owing to charge neutralization, while very high charge ratios do not provide enough charges to permit an interaction that induces nanoparticle formation. Overall, it was demonstrated that by modulating charge ratios, the final properties of CS/CRG/TPP nanoparticles can be adjusted to specific applications.

Taking into account the small size and high positive charge displayed by the developed nanosystems, they are considered to hold potential for an application in mucosal delivery of macromolecules.

Acknowledgements

This work was supported by National Portuguese funding through FCT - Fundação para a Ciência e a Tecnologia, project PEst-OE/EQB/LA0023/2011 and PTDC/SAU-FCF/100291/2008. The authors thank Carmen Serra from C.A.C.T.I., University of Vigo, Spain, for the helpful analysis of XPS and TOF-SIMS results.

References

Adekogbe, I., & Ghanem, A. (2005). Fabrication and characterization of DTBP-crosslinked chitosan scaffolds for skin tissue engineering. *Biomaterials*, *26*(35), 7241–7250.

Al-Qadi, S., Grenha, A., & Remuñán-López, C. (2011). Microspheres loaded with polysaccharide nanoparticles for pulmonary delivery: Preparation, structure and surface analysis. *Carbohydrate Polymers*, *86*(1), 25–34.

Allott, T. E. H., Curtis, C. J., Hall, J., Harriman, R., & Battarbee, R. W. (1995). The impact of nitrogen deposition on upland surface waters in Great Britain: A regional assessment of nitrate leaching. *Water, Air, & Soil Pollution*, *85*(2), 297–302.

Baltrusaitis, J., Jayaweera, P. M., & Grassian, V. H. (2009). XPS study of nitrogen dioxide adsorption on metal oxide particle surfaces under different environmental conditions. *Physical Chemistry Chemical Physics*, *11*(37), 8295–8305.

Barnes, T. J., Kempson, I. M., & Prestidge, C. A. (2011). Surface analysis for compositional, chemical and structural imaging in pharmaceutics with mass spectrometry: A ToF-SIMS perspective. *International Journal of Pharmaceutics*, *417*(1–2), 61–69.

Barr, T. L., & Seal, S. (1995). Nature of the use of adventitious carbon as a binding-energy standard. *Journal of Vacuum Science & Technology A: Vacuum Surfaces and Films*, *13*(3), 1239–1246.

Bixler, H. J. (1993). The carrageenan connection IV. *British Food Journal*, *96*, 12–17.

Briggs, D., & Seah, M. P. (1983). *Practical surface analysis by Auger and X-ray photoelectron spectroscopy*. New York: John Wiley & Sons.

Calvo, P., Remuñán-López, C., Vila-Jato, J. L., & Alonso, M. J. (1997a). Novel hydrophilic chitosan-polyethylene oxide nanoparticles as protein carriers. *Journal of Applied Polymer Science*, *63*(1), 125–132.

Calvo, P., Remuñán-López, C., Vila-Jato, J. L., & Alonso, M. J. (1997b). Chitosan and chitosan/ethylene oxide-propylene oxide block copolymer nanoparticles as novel carriers for proteins and vaccines. *Pharmaceutical Research*, *14*(10), 1431–1436.

Chen, Y., Mohanraj, V. J., Wang, F., & Benson, H. A. E. (2007). Designing chitosan–dextran sulfate nanoparticles using charge ratios. *AAPS PharmSciTech*, *8*(4), 131–139.

Crouzier, T., & Picart, C. (2009). Ion pairing in polyelectrolyte multilayer films containing polysaccharides. *Biomacromolecules*, *10*(2), 433–442.

de la Fuente, M., Csaba, N., Garcia-Fuentes, M., & Alonso, M. J. (2008). Nanoparticles as protein and gene carriers to mucosal surfaces. *Nanomedicine*, *3*(6), 845–857.

Desai, M. P., Labhasetwar, V., Amidon, G. L., & Levy, R. J. (1996). Gastrointestinal uptake of biodegradable microparticles: Effect of particle size. *Pharmaceutical Research*, *13*(12), 1838–1845.

Dornish, M., Hagen, A., Hansson, E., Peucheur, C., Vedier, F., & Skaugrud, O. (1997). *Safety of Protasan™: Ultrapure chitosan salts for biomedical and pharmaceutical use*. Lyon: Jacques Andre publisher.

Edwards, I. P., Zak, D. R., Kellner, H., Eisenlord, S. D., & Pregitzer, K. S. (2011). Simulated atmospheric N deposition alters fungal community composition and suppresses ligninolytic gene expression in a northern hardwood forest. *Plos One*, *6*(6), e20421.

Fernández-Urrusuno, R., Calvo, P., Remuñán-López, C., Vila-Jato, J. L., & José Alonso, M. (1999). Enhancement of nasal absorption of insulin using chitosan nanoparticles. *Pharmaceutical Research*, *16*(10), 1576–1581.

Grenha, A. (2012). Chitosan nanoparticles: A survey of preparation methods. *Journal of Drug Targeting*, doi:10.3109/1061186X.2011.654121

Grenha, A., Gomes, M. E., Rodrigues, M., Santo, V. E., Mano, J. F., Neves, N. M., & Reis, R. L. (2010). Development of new chitosan/carrageenan nanoparticles for drug delivery applycations. *Journal of Biomedical Materials Research A*, *92A*, 1265–1272.

Grenha, A., Remuñán-López, C., Carvalho, E. L., & Seijo, B. (2008). Microspheres containing lipid/chitosan nanoparticles complexes for pulmonary delivery of therapeutic proteins. *European Journal of Pharmaceutics and Biopharmaceutics*, *69*(1), 83–93.

Grenha, A., Seijo, B., Serra, C., & Remuñán-López, C. (2007). Chitosan nanoparticle-loaded mannitol microspheres: Structure and surface characterization. *Biomacromolecules*, *8*(7), 2072–2079.

Hirano, S., Seino, H., Akiyama, Y., & Nonaka, I. (1988). Biocompatibility of chitosan by oral and intravenous administrations. *Polymer Materials and Science Engineering*, *59*, 897–901.

Janes, K. A., Calvo, P., & Alonso, M. J. (2001). Polysaccharide colloidal particles as delivery systems for macromolecules. *Advanced Drug Delivery Reviews*, *47*(1), 83–97.

Jani, P., Halbert, G. W., Langridge, J., & Florence, A. T. (1990). Nanoparticle uptake by the rat gastrointestinal mucosa: Quantitation and particle size dependency. *Journal of Pharmacy and Pharmacology*, *42*(12), 821–826.

Jiang, W., Saxena, A., Song, B., Ward, B. B., Beveridge, T. J., & Myneni, S. C. B. (2004). Elucidation of functional groups on Gram-positive and Gram-negative bacterial surfaces using infrared spectroscopy. *Langmuir*, *20*, 11433–11442.

Lehr, C. M., Bouwstra, J. A., Schacht, E. H., & Junginger, H. E. (1992). In vitro evaluation of mucoadhesive properties of chitosan and some other natural polymers. *International Journal of Pharmaceutics*, *78*(1–3), 43–48.

Lim, Y. M., Gwon, H. J., Choi, J. H., Shin, J., & Nho, Y. C. (2010). Preparation and biocompatibility study of gelatin/kappa-carrageenan scaffolds. *Macromolecular Research*, *18*, 29–34.

Liu, Z., Jiao, Y., Wang, Y., Zhou, C., & Zhang, Z. (2008). Polysaccharides-based nanoparticles as drug delivery systems. *Advanced Drug Delivery Reviews*, *60*, 1650–1662.

López-León, T., Carvalho, E. L. S., Seijo, B., Ortega-Vinuesa, J. L., & Bastos-González, D. (2005). Physicochemical characterization of chitosan

nanoparticles:electrokinetic and stability behavior. *Journal of Colloid and Interface Science*, *283*, 344–351.
Ma, O., Lavertu, M., Sun, J., Nguyen, S., Buschmann, M. D., Winnik, F. M., & Hoemann, C. D. (2008). Precise derivatization of structurally distinct chitosans with rhodamine B isothiocyanate. *Carbohydrate Polymers*, *72*, 616–624.
Malafaya, B. M., Silva, A. G., & Reis, R. L. (2007). Natural-origin polymers as carriers and scaffolds for biomolecules and cell delivery in tissue engineering applications. *Advanced Drug Delivery Reviews*, *59*, 207–233.
Mi, F. L., Sung, H. W., Shyu, S. S., Su, C. C., & Peng, C. K. (2003). Synthesis and characterization of biodegradable TPP/genipin co-crosslinked chitosan gel beads. *Polymer*, *44*(21), 6521–6530.
Mohamadnia, Z., Zohuriaan-Mehr, M. J., Kabiri, K., Jamshidi, A., & Mobedi, H. (2007). pH-sensitive IPN hydrogel beads of carrageenan-alginate for controlled drug delivery. *Journal of Bioactive and Compatible Polymers*, *22*, 342–356.
Mohanraj, V. J., & Chen, Y. (2006). Nanoparticles—A review. *Tropical Journal of Pharmaceutical Research*, *5*, 561–573.
Nizri, G., Magdassi, S., Schmidt, J., Cohen, Y., & Talmon, Y. (2004). Microstructural characterization of micro- and nanoparticles formed by polymer–surfactant interactions. *Langmuir*, *20*(11), 4380–4385.
Nizri, G., Makarsky, A., Magdassi, S., & Talmon, Y. (2009). Nanostructures formed by self-assembly of negatively charged polymer and cationic surfactants. *Langmuir*, *25*(4), 1980–1985.
Rao, C. N. R., Rao, G. R., & Ppabhakaran, K. (1987). A combined XPS-UPS-EELS study of nitrogen adsorbed on clean and barium-promoted iron surfaces: The nature of the precursor to dissociation. *Chemical Physics Letters*, *134*(1), 47–50.
Rawat, M., Singh, D., & Saraf, S. (2006). Nanocarriers: Promising vehicle for bioactive drugs. *Biological & Pharmaceutical Bulletin*, *29*(9), 1790–1798.
Reis, C., & Ribeiro, A. (2006). Nanoencapsolation II. Biomedical applications and current status of peptide and protein nanoparticulate delivery systems. *Nanomedicine: Nanotechnology Biology and Medicine*, *2*, 53–65.
Saboktakin, M. R., Tabatabaie, R. M., Maharramov, A., & Ramazanov, M. A. (2010). Synthesis and characterization of superparamagnetic chitosan–dextran sulphate hydrogels as nano carriers for colon-specific drug delivery. *Carbohydrate Polymers*, *81*, 372–376.
Silva, S. S., Luna, S. M., Gomes, M. E., Benesch, J., Pashkuleva, I., Mano, J. F., & Reis, R. L. (2008). Plasma surface modification of chitosan membranes: Characterization and preliminary cell response studies. *Macromolecular Bioscience*, *8*(6), 568–576.
Sung, H. W., Huang, D. M., Chang, W. H., Huang, R. N., & Hsu, J. C. (1999). Evaluation of gelatin hydrogel crosslinked with various crosslinking agents as bioadhesives: In vitro study. *Journal of Biomedical Materials Research*, *46*(4), 520–530.
Swift, P. (1982). Adventitious carbon—The panacea for energy referencing. *Surface and Interface Analysis*, *4*(2), 47–51.
van de Velde, F., Knutsen, S. H., Usov, A. I., Rollemay, H. S., & Cerezo, A. S. (2002). 1H and13C high resolution NMR spectroscopy of carrageenans:application, research and industry. *Trends in Food Science & Technology*, *13*, 73–92.
Wilson, R. H., Smith, A. C., Kacurakova, M., Saunders, P. K., Wellner, N., & Waldron, K. W. (2000). The mechanical properties and molecular dynamics of plant cell wall polysaccharides studied by Fourier-transform infrared spectroscopy. *Plant Physiology*, *124*(1), 397–405.